Inhomogeneous dynamics in confined water nanodroplets

Adriaan M. Dokter*, Sander Woutersen, and Huib J. Bakker

FOM-Institute for Atomic and Molecular Physics, Kruislaan 407, 1098 SJ, Amsterdam, The Netherlands

Edited by F. Fleming Crim, University of Wisconsin, Madison, WI, and approved August 21, 2006 (received for review April 24, 2006)

The effect of confinement on the dynamical properties of liquid water was studied by mid-infrared ultrafast pump–probe spectroscopy on HDO:D_2O in reverse micelles. By preparing water-containing reverse micelles of different well defined sizes, we varied the degree of geometric confinement in water nanodroplets with radii ranging from 0.2 to 4.5 nm. We find that water molecules located near the interface confining the droplet exhibit slower vibrational energy relaxation and have a different spectral absorption than those located in the droplet core. As a result, we can measure the orientational dynamics of these different types of water with high selectivity. We observe that the water molecules in the core show similar orientational dynamics as bulk water and that the water layer solvating the interface is highly immobile.

AOT | confinement | infrared | mid-infrared pump–probe spectroscopy | reverse micelle

There are many examples in the fields of biology (1, 2), geochemistry (3), tribology (4), and nanofluidics (5), where water molecules are not present as a bulk liquid, but in small numbers and confined geometries. The presence of an interface is known to influence the structure and dynamics of liquid water. Near a surface, ordering of water molecules into layers occurs (6–8), as was shown by steady-state surface-sensitive techniques like x-ray diffraction. This ordering was found to extend up to several molecular diameters into the liquid. In the case of small water droplets, the confinement is three-dimensional, and the overall structure and dynamics of the water may be affected.

A suitable model system for studying confined water nanodroplets are reverse micelles (9, 10). A solution of nanometer-sized droplets forms when preparing an emulsion of water in an apolar solvent by addition of a surfactant. The anionic lipid surfactant sodium bis(2-ethylhexyl) sulfosuccinate (AOT) is known to form micelles that are reasonably monodisperse (≈15%) (11, 12). The size of the water droplets can be easily varied by changing the molar water-to-AOT ratio, conventionally denoted by the parameter $w_0 = [H_2O]/[AOT]$.

In previous studies, two-component models have been proposed to describe both the linear absorption (13) and the vibrational energy relaxation (14, 15) of confined water, to reflect the different properties of water located at the surface and in the core of the nanodroplets. As for the structural hydrogen bond rearrangements of liquid water, the effects of nanoconfinement are under much debate. So far, no inhomogeneities were observed in the molecular orientational motions of the water molecules throughout the droplets (14), although such inhomogeneities have been predicted by molecular dynamics simulations (16). A decrease in the average mobility of water in nanodroplets has been observed by several techniques (17–20), although so far no distinction could be made between water molecules at the surface layers of the droplets and those in the core. Therefore, from these studies it remained unclear whether the mobility of water in nanodroplets decreases overall, or whether molecules located near the surface and in the core of the droplets show different dynamical behavior. Here, we use spectrally resolved ultrafast mid-infrared pump–probe spectroscopy on the O–H stretch vibration of isotopically diluted water (HDO in D_2O) contained in reverse micelles. In these experiments, we observe separately the contributions of core and interfacial water molecules, and find that the molecular mobilities are surprisingly different.

Results and Discussion

The structural dynamics of water can be studied through the dynamics of the OH-stretch vibrational frequencies of the molecules, because these frequencies strongly correlate with the strength of the hydrogen bonds (21, 22). Compared with bulk water, we find the hydrogen bond dynamics of confined water to be strikingly different. We measured the transient spectral response of both bulk water and a $w_0 = 7$ micelle ($n_{water} \approx 425$) when pumping at the blue wing of the OH-stretch spectrum (mainly exciting weakly hydrogen-bonded molecules), and at the red wing (mainly exciting strongly hydrogen-bonded molecules). The pump-induced transmission changes at 2-ps time delay are shown in Fig. 1 as a transient pump–probe spectrum.

From Fig. 1 *Left*, we see that for bulk water, irrespective of which subset of water molecules was initially excited, the pump–probe spectra become identical very rapidly (within 1 ps). This fast spectral diffusion shows that rapid fluctuations within the hydrogen bond network cause a fast interconversion of strong and weak hydrogen bonds (23, 24). As a result, the excited subset of molecules quickly reaches its spectral equilibrium distribution. This finding sharply contrasts with the case of water confined in a nanodroplet, as shown in Fig. 1 *Right*. Here, the pump–probe spectra obtained with different pump frequencies remain shifted relatively, even at long delays (≫10 ps). The confined liquid apparently contains spectrally separated subsets of OH oscillators that do not interchange their absorption frequencies on a picosecond time scale, which implies that water molecules within the nanodroplets experience different local hydrogen bonding over long time scales.

The observed inhomogeneity in the dynamics of the confined water molecules can be further investigated by studying their vibrational relaxation, which is known to depend strongly on the local hydrogen bonding (21). In recent studies on pure (not isotopically diluted) water, it was shown that the vibrational relaxation rate increases with micelle size (15, 25). However, this work could only reveal the average dynamics of the water molecules, because of the rapid intermolecular energy transfer (25, 26). Fig. 2 shows the vibrational relaxation we measured for isotopically diluted water in nanodroplets. The decay is clearly multiexponential (as opposed to bulk HDO in D_2O) and dependent on micelle size. We find from a global fit to all delay curves of measurements on seven samples of different micelle sizes (32 probe frequencies per sample), that the dynamics can

Author contributions: S.W. and H.J.B. designed research; A.M.D., S.W., and H.J.B. performed research; and A.M.D. wrote the paper.

The authors declare no conflict of interest.

This article is a PNAS direct submission.

Freely available online through the PNAS open access option.

*To whom correspondence should be addressed. E-mail: a.dokter@amolf.nl.

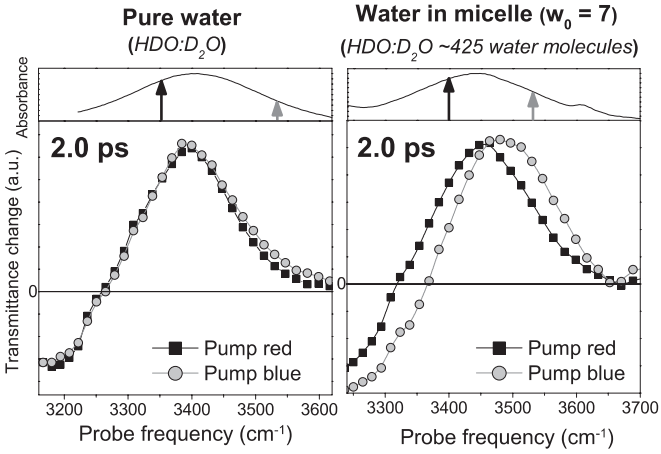

Fig. 1. Comparison of the transient pump–probe spectrum at 2 ps of confined water in a reverse micelle and bulk water, when selectively pumping different spectral subsets (pump frequencies indicated by the vertical arrows in the conventional absorption spectra).

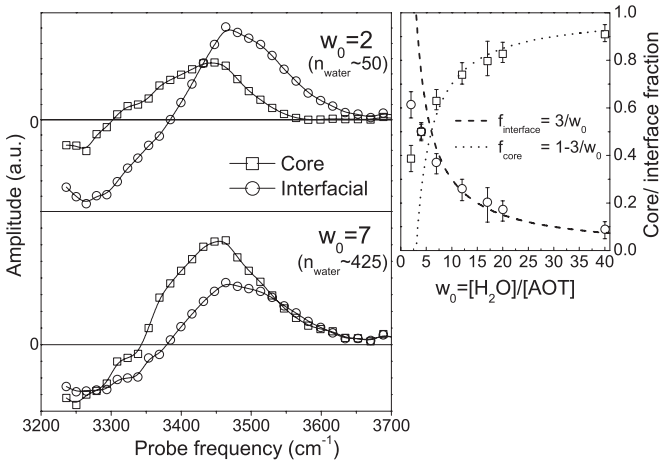

Fig. 3. Spectral amplitudes of the core (fast) and interfacial (slow) components in the vibrational relaxation for water in two sizes of reverse micelles, obtained from a global fit to the data. (*Right*) The relative core and interfacial fractions, which are obtained by spectrally integrating the positive (bleaching) part of the spectrum for each of the two components. Error bars are put at those fractions where the χ^2 value of the global fit doubles its minimized value (keeping the interfacial vibrational lifetime fixed).

be well described by a model of two components with different vibrational relaxation time constants T_1 (see *Supporting Text*, Table 1, and Figs. 5 and 6, which are published as supporting information on the PNAS web site). Although we observe a slight frequency dependence in the relaxation rate of the slow component, we did not include it to limit the number of fit parameters. In the fit, the relative amplitudes of each component may vary both with absorption frequency and size of the reverse micelle. Fig. 3 shows the obtained spectral amplitudes for two sizes of micelles. The blue-shifted component has $T_1 = 2.8$ ps for all droplet sizes. For the red-shifted component, T_1 decreases from 1.0 ps for the smallest droplet to 0.7 ps for the largest droplet.

As we lower the surface-to-volume ratio of the water droplets by increasing their size, the amplitude of the slow component in the vibrational relaxation strongly decreases, as illustrated in Fig. 3 *Right*. For micelles having $w_0 > 10$, we find a decrease of the relative fraction of the slow component f_{slow} consistent with a $1/w_0$ dependence on the parameter w_0 ($\propto w_0^{-\alpha}$, $\alpha = 0.85 \pm 0.25$). Because the micelle radius varies linearly with w_0 in this size regime (12), the fraction of the slow component is in fact inversely proportional to the radius of the droplet, just like the surface-to-volume ratio of a sphere. This finding strongly suggests that the slow component is associated with water molecules at the droplet interface. Assuming a dependence of the slow component proportional to $1/w_0$, we find a prefactor to this term of 3.3 ± 0.3. If we neglect differences in the absorption cross-section of the core and interfacial molecules, this factor suggests a surface coordination of six to seven hydrogen bonds per surfactant molecule (an interfacial fraction of 1 would occur at $w_0 \approx 3$, i.e., three water molecules or six hydrogen bonds per AOT molecule). This number of hydrogen bonds is consistent with the fact that there are the six lone electron pairs located at the oxygens of the sulfonate anion of the AOT surfactant molecule, which can accept one hydrogen bond each. We thus assign the slow component to interfacial water and the fast component to core water.

For the smaller micelles ($w_0 < 10$), we observe that the amplitude of the interfacial component does not follow a $1/w_0$ proportionality, but increases more slowly with decreasing w_0. This deviation is also found in molecular dynamics simulations (16). In fact, for all micelles studied, the size-dependence of the interfacial component we observe agrees well with the calculated number of molecules within the first solvation layer of the micelle cavity.† The simulations show that, for the smallest micelles, the interface is strongly curved, and the surfactant molecules are less hydrated and pack more closely. Therefore, the density of water molecules located at the interface decreases, explaining the deviation from the approximate $3/w_0$-dependence for the smaller micelles ($w_0 < 10$).

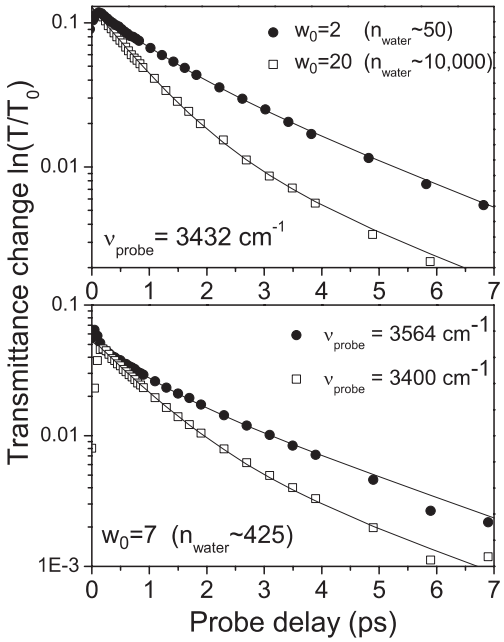

Fig. 2. Pump-induced transmission change at the OH-stretch absorption, plotted as a function of probe delay for two droplet sizes at a single probe frequency (*Upper*) and at different probe frequencies for a single droplet size (*Lower*). The pump wavelength was kept constant at 3,480 cm^{-1}.

†Faeder and Ladanyi (16) define the interfacial fraction as those molecules located within 0.5 nm of the reverse micelle cavity boundary. The present work shows the same micelle size-dependence for this fraction, but by an absolute fraction 20% lower, likely because it does not include any OH groups forming hydrogen bonds to other water molecules.

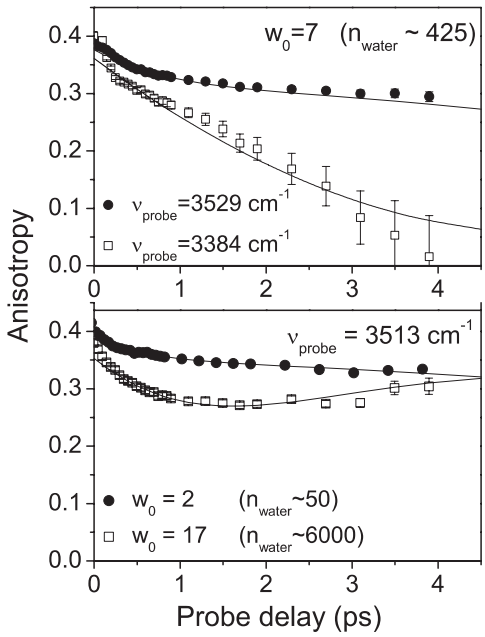

Fig. 4. Comparison of the anisotropy decay of the OH-stretch vibration at two different probe frequencies for an intermediate size micelle of $w_0 = 7$ (*Upper*), and a comparison of the orientational relaxation for two different reverse micelle sizes ($w_0 = 2,17$) at a single probe wavelength of 3,513 cm^{-1} (*Lower*).

The spectrum of the interfacial component is blue-shifted with respect to the core component, as seen in Fig. 3, which points to a weakening of the hydrogen bonds of these molecules (25). The OH···O hydrogen bond is known to weaken if it is not parallel to the OH bond (22, 27), and this configuration is likely to occur at a micellar interface. The local binding structure of the interfacial water depends on the hydrophilic interactions with the surfactant molecules and their counterions (28) and on packing constraints. The near-tetrahedral hydrogen-bond network that exists for bulk water will be disrupted at the interface, resulting in poorly directional and possibly even bifurcated hydrogen bonds.

The core water molecules have an average hydrogen-bonding that is slightly weaker compared with bulk water, as can be concluded from the missing red wing in the spectrum of the core component. This red wing recovers in going from $w_0 = 12$ to 40, and the vibrational relaxation rate approaches the bulk value only at about $w_0 = 40$. Therefore, water with full bulk-like character only starts to appear in a cluster of at least 2,000 water molecules ($w_0 = 12$) and bulk-like molecules fully dominate the dynamics over molecules with interfacial character at clusters >80,000 molecules ($w_0 = 40$). Note that the sodium counterions of the AOT surfactant molecules are not expected to have a large influence on the dynamics of the core component, because they mainly associate with the anionic headgroups and are only partly solvated (28). In addition, it is has been found that the effect of sodium cations on the dynamics of bulk water is very small (29).

To obtain information on the molecular motions of the core and interfacial water, we measured the decay of the anisotropy in the orientation of the pump-excited OH-groups. Preferentially, OH-stretch oscillators parallel to the pump polarization will absorb, causing different transmissions for probe light polarized parallel and perpendicular to the pump polarization. The decay of the relative difference of these two signals gives direct information on the angular motions of the OH-groups of the water molecules.

Fig. 4 shows four anisotropy decay curves for different absorption frequencies and micelle sizes. When the interfacial component dominates, which is the case at the blue absorption frequencies of especially the smallest nanodroplets, the anisotropy parameter decays very slowly with a time constant of >20 ps. The water layer solvating the interface is apparently highly immobile, despite the fact that these molecules are more weakly hydrogen bonded than those located in the micelle center. At frequencies where the core component dominates, the anisotropy decays rapidly on a time scale of a few picoseconds. For example, this is the case for the decay curve shown in Fig. 4 for a $w_0 = 7$ micelle at 3,384 cm^{-1}, which is the absorption frequency at the zero-crossing of the pump–probe signal of the interfacial water molecules (see Fig. 3).

A quite peculiar anisotropy decay can be observed at frequencies where we find both core and interfacial water, as illustrated by the decay curve for the $w_0 = 17$ micelle in Fig. 4. Directly after excitation, we observed an anisotropy decay with an associated time constant close to that of bulk water, but the decay quickly levels off and even rises from ≈2 ps onward. This effect can be understood in terms of the different vibrational relaxation time-constants associating core and interfacial water. Because only excited molecules contribute to the observed anisotropy and the vibrations of the interfacial water decay more slowly, the relative contribution of interfacial water to the signal will increase in time. As time progresses, the anisotropy parameter increasingly reflects the slowly decaying anisotropy of the interfacial molecules. This observation explains the recovery of the value of the anisotropy parameter at later delays.

The observed anisotropy curves can be well described by a model in which the previously determined core and interfacial water fractions have different reorientational time constants, as shown by the curves in Fig. 4 obtained from a global fit. We find that the core water reorients on a time scale close to that of bulk water (2–4 ps) (24, 30), whereas the interfacial water is highly immobile (>15 ps).

In recent anisotropy relaxation measurements on the OD hydroxyl stretch of water by Piletic and colleagues (14, 18), it was also found that the orientational mobility of the molecules strongly changes when the micelle size decreases. However, Piletic and colleagues did not observe an inhomogeneity in the orientational relaxation throughout the droplet, and concluded that the hydrogen bond structural rearrangements of confined water are best described within a framework in which all molecules are treated equivalently. These conclusions contrast our observations presented above. A possible reason that the orientational motions of the two sorts of water can be distinguished in this study is the experimental advantage that we measure the dynamics spectrally resolved over the entire frequency range of the OH-stretch absorption band. The competition between the core and interfacial contributions to the anisotropy is most obvious in larger micelles at relatively blue absorption frequencies. In these cases, one can observe most clearly the transition from a case in which the anisotropy is dominated by a large amount of core molecules, to a case in which the interfacial molecules dominate at later delays in view of their longer vibrational lifetime and blue absorption frequency (see Fig. 4). In addition, the OH band is more strongly inhomogeneously broadened than the OD band, which allows for a better spectral distinction of different species, i.e., the water in the core and at the interface of the micelle.

The observation of slow orientational dynamics for the interfacial water molecules is supported by recent molecular dynamics simulations on micellar systems (16, 31). These studies have suggested that water molecules can remain bound to micellar surfaces for >100 ps. Other calculations show that the ionic–dipole interaction between the surfactant and its solvating water molecules is strong (32), leading to a local ordering and density increase of water molecules close to the surfactant molecules

(16). Also, the sodium counterions, which mainly associate with the sulfonate anionic headgroups at the interface, will influence the dynamical properties of neighboring water (28).

Core and interfacial water molecules show strongly different orientational mobilities, which has to be explained from their different intermolecular interactions and very different geometric arrangements. Molecular reorientation involves the subsequent breaking and formation of hydrogen bonds. Interestingly, the activation energy for this process is not the same as the hydrogen bond binding energy, as is apparent from the fact that interfacial water has a smaller hydrogen bond binding energy, yet shows a slower molecular reorientation. For core water molecules (as for bulk water), the activation energy for reorientation is substantially lowered, because these molecules can break a hydrogen bond while simultaneously forming a new bond with another water molecule (33). For interfacial water, this process is inhibited because these molecules are hydrogen bonded to a heavy immobile surfactant molecule. Because of this geometric effect, weakly hydrogen bonded molecules can experience a slow reorientation and slow hydrogen bond dynamics, even though their hydrogen bond binding energy is relatively small.

In conclusion, we studied the vibrational and rotational dynamics of water molecules contained in water nanodroplets using femtosecond transient vibrational spectroscopy. We find that we can distinguish core and interfacial water on the basis of their different vibrational lifetimes. The orientational motions of the water molecules turn out to be strongly inhomogeneous in the droplet. Even for small micelles, the water molecules in the core reorient on a similar time-scale as bulk liquid water. Therefore, nano-confinement has a negligible effect on the orientational mobility of water molecules in the core of the droplets. We find the water at the interface to be highly immobile, despite the fact that their hydrogen bonding is weaker compared with molecules in the core of the droplets.

Materials and Methods

Reverse micelle samples were studied with droplet radii of 0.2–4.5 nm, corresponding to clusters of 50–80,000 water molecules (w_0 = 2, 4, 7, 12, 17, 20, 40). We performed ultrafast mid-infrared pump–probe spectroscopy on the OH stretch vibration of diluted HDO in D_2O. In the experiment, a first intense mid-infrared light pulse excites a spectral subset of OH oscillators, inducing transmission changes for a weak second time-delayed probe pulse. After excitation, the transmission is increased at frequencies matching the $\nu_{OH} = 0 \rightarrow 1$ transition (because of ground state depletion of the OH stretch vibration and stimulated emission out of the $v = 1$ state), whereas the transmission is decreased at the more red-shifted frequencies matching the $\nu_{OH} = 1 \rightarrow 2$ transition (where the induced population in the $v = 1$ state causes an absorption).

The transmitted probe beam is split into components polarized parallel ($s_{\parallel}$) and perpendicular ($s_{\perp}$) with respect to the pump polarization, and both components are spectrally resolved on a nitrogen-cooled HgCdTe detector array by using a polychromator. The average of the two polarization components ($s_{\parallel} + 2s_{\perp}$) gives an absorption change that represents the frequency-resolved relaxation of the OH-stretch vibration. From the relative difference between the polarization components ($(s_{\parallel} - s_{\perp})/(s_{\parallel} + 2s_{\perp})$), we construct the anisotropy decay, which gives information on the molecular orientational motions.

Because of heating of the sample caused by the intense pump pulse, we measure a small thermal signal (0.1–5% of the total transmission change, depending on frequency and micelle size) in the pump-induced absorbance changes. This signal is modeled to grow in at the vibrational relaxation rate to the level of absorption change that is measured at ≈10 times the average vibrational relaxation time constant for each micelle (i.e., at 20, 15, 12, 10, 10, 9, and 9 ps for w_0 = 2, 4, 7, 12, 17, 20, and 40, respectively). At these delay times, the population-induced transmission changes are negligible and only the thermal signal is present. This signal is subsequently subtracted from the original signal. We do not take into account the slow decay of the thermal signal due to cooling of the micelle to its surroundings (12). For this approximation to be valid, we performed experiments on highly diluted samples of of HDO in D_2O (H_2O/D_2O = 1:40). In this case, the heating of the micelles is very limited and the subsequent cooling very slow, making the thermal signal effectively constant over the time window considered; subtracting the thermal signal at 15 times the average vibrational relaxation time instead of 10 did not lead to any significant change of the fit parameters obtained at the later time. Isotopically diluted water samples are necessary as well to prevent the signals to be affected by intermolecular resonant energy transfer of the OH stretch vibrations.

We thank L. Kuipers and J. L. Herek for critically reading the manuscript and H. Schoenmaker for technical support. This work is part of the research program of the "Stichting voor Fundamenteel Onderzoek der Materie (FOM)", which is financially supported by the "Nederlandse organisatie voor Wetenschappelijk Onderzoek (NWO)."

1. Otting G, Liepinsh E, Wuthrich K (1991) *Science* 254:974–980.
2. Pal SK, Peon J, Zewail AH (2002) *Proc Natl Acad Sci USA* 99:1763–1768.
3. Sposito G, Skipper NT, Sutton R, Park S-H, Soper AK, Greathouse JA (1999) *Proc Natl Acad Sci USA* 96:3358–3364.
4. Bhushan B, Israelachvili JN, Landman U (1995) *Nature* 374:607–616.
5. Raviv U, Laurat P, Klein J (2001) *Nature* 413:51–54.
6. Toney MF, Howard JN, Richer J, Borges GL, Gordon JG, Melroy OR, Wiesler DG, Yee D, Sorensen LB (1994) *Nature* 368:444–446.
7. Reedijk MF, Arsic J, Hollander FFA, de Vries SA, Vlieg E (2003) *Phys Rev Lett* 90:066103.
8. Cheng L, Fenter P, Nagy KL, Schlegel ML, Sturchio NC (2001) *Phys Rev Lett* 87:156103.
9. Levinger NE (2002) *Science* 298:1722–1723.
10. Deak JC, Pang Y, Sechler TD, Wang Z, Dlott DD (2004) *Science* 306:473–476.
11. Abel S, Sterpone F, Bandyopadhyay S, Marchi M (2004) *J Phys Chem B* 108:19458–19466.
12. Seifert G, Patzlaff T, Graener H (2002) *Phys Rev Lett* 88:147402.
13. Fioretto D, Freda M, Onori G, Santucci A (1999) *J Phys Chem B* 103:2631–2635.
14. Piletic IR, Moilanen DE, Spry DB, Levinger NE, Fayer M (2006) *J Phys Chem A* 110:4985–4999.
15. Cringus D, Lindner J, Milder MTW, Pshenichnikov MS, Voehringer P, Wiersma DA (2005) *Chem Phys Lett* 408:162–168.
16. Faeder J, Ladanyi BM (2000) *J Phys Chem B* 194:1033–1046.
17. Harpham MR, Ladanyi BM, Levinger NE (2004) *J Chem Phys* 121:7855–7868.
18. Tan H-S, Piletic IR, Fayer M (2005) *J Chem Phys* 122:174501.
19. Willard DM, Riter RE, Levinger NE (1198) *J Am Chem Soc* 120, 4151–4160.
20. Scodinu A, Fourkas JT (2002) *J Phys Chem B* 106:10292–10295.
21. Lawrence CP, Skinner JL (2003) *J Chem Phys* 118:264–272.
22. Rey R, Møller KB, Hynes JT (2002) *J Phys Chem B* 106:11993–11996.
23. Gale A, Gallot G, Hache F, Lascoux N, Bratos S, Leicknam J (1999) *Phys Rev Letters* 82:1068–1071.
24. Nienhuys H-K, van Santen RA, Bakker HJ (2000) *J Chem Phys* 112:8487–8494.
25. Dokter AM, Woutersen S, Bakker HJ (2005) *Phys Rev Lett* 94:178301.
26. Cowan ML, Bruner BD, Huse N, Dwyer JR, Chugh B, Nibbering ETJ, Elsaesser T, Miller RJD (2005) *Nature* 434:199–202.
27. Walrafen GE (1979) *J Chem Phys* 52:4176–4198.
28. Harpham MR, Ladanyi BM, Levinger NE (2005) *J Phys Chem B* 109:16891–16900.
29. Omta AW, Kropman MF, Woutersen S, Bakker HJ (2003) *Science* 301:347–349.
30. Fecko CJ, Loparo JJ, Roberts ST, Tokmakoff A (2005) *J Chem Phys* 122:054506.
31. Balasubramanian S, Pal S, Bagchi B (2002) *Phys Rev Lett* 89:115505.
32. Derecskei B, Derecskei-Kovacs A, Schelly Z (1999) *Langmuir* 15:1981–1992.
33. Laage D, Hynes J (2006) *Science* 311:832–835.